6234 *Biochemistry* **2010,** *49,* 6234–6246
DOI: 10.1021/bi1000118

BIOCHEMISTRY
including biophysical chemistry & molecular biology
Article

Kinetic Evidence for the Sequential Association of Insulin Binding Sites 1 and 2 to the Insulin Receptor and the Influence of Receptor Isoform[†,‡]

Karina Sinding Thorsøe, Morten Schlein, Dorte Bjerre Steensgaard, Jakob Brandt, Gerd Schluckebier, and Helle Naver*

Diabetes Protein Engineering, Novo Nordisk A/S, Novo Nordisk Park, 2760 Maløv, Denmark

Received January 6, 2010; Revised Manuscript Received June 17, 2010

ABSTRACT: Through binding to and signaling via the insulin receptor (IR), insulin is involved in multiple effects on growth and metabolism. The current model for the insulin−IR binding process is one of a biphasic reaction. It is thought that the insulin peptide possesses two binding interfaces (sites 1 and 2), which allow it to bridge the two α-subunits of the insulin receptor during the biphasic binding reaction. The sequential order of the binding events involving sites 1 and 2, as well as the molecular interactions corresponding to the fast and slow binding events, is still unknown. In this study we examined the series of events that occur during the binding process with the help of three insulin analogues: insulin, an analogue mutated in site 2 (B17A insulin), and an analogue in which part of site 1 was deleted (Des A1−4 insulin), both with and without a fluorescent probe attached. The binding properties of these analogues were tested using two soluble Midi IR constructs representing the two naturally occurring isoforms of the IR, Midi IR-A and Midi IR-B. Our results showed that in the initial events leading to Midi IR−insulin complex formation, insulin site 2 binds to the IR in a very fast binding event. Subsequent to this initial fast phase, a slower rate-limiting phase occurs, consistent with a conformational change in the insulin−IR complex, which forms the final high-affinity complex. The terminal residues A1−A4 of the insulin A-chain are shown to be important for the slow binding phase, as insulin lacking these amino acids is unable to induce a conformational change of IR and has a severely impaired binding affinity. Moreover, differences in the second phase of the binding process involving insulin site 1 between the IR-A and IR-B isoforms suggest that the additional amino acids encoded by exon 11 in the IR-B isoform influence the binding process.

Insulin has long been known to exert multiple effects through hormonal control of metabolism. Central to these effects is the interaction between insulin and the extracellular domain of the insulin receptor (IR).[1] This binding initiates a signaling cascade, which is not only pivotal for controlling blood glucose levels (*1*) and glucose disposal in muscle and adipose tissue but also important in controlling protein synthesis and cell growth and survival in addition to male sex determination. A dysfunctional interaction between IR and insulin results in a lack of intracellular signaling and has been implicated in severe diseases such as type 2 diabetes and cancer (*2*). A significant effort has been put into understanding IR recognition by insulin at the molecular level; however, the mechanism by which insulin binding triggers the insulin response is still not fully understood.

Insulin is a globular protein consisting of two polypeptide chains, A and B (21 and 30 amino acid residues, respectively), which are linked by two disulfide bridges. The three-dimensional structure of insulin has been described by both X-ray crystallography and NMR spectroscopy (*3*−*6*). A number of amino acid residues have been implicated in the binding of insulin to the IR, and these amino acid residues are grouped into two sites: The classical binding site, site 1 (*7*), which primarily consists of Gly A1, Ile A2, Val A3, Asn A4, Tyr A19, Val B12, Phe B24, and Phe B25. Amino acid residues Gln A5, Asn A21, Tyr B16, Gly B23, and Tyr B26 also contribute (*8*). The second binding site, site 2, involving amino acid residues Leu A13 and Leu B17 is positioned opposite site 1 (*7*). Data indicate that in the IR−insulin binding process, the B-chain of insulin is displaced, thereby exposing Ile A2 and Val A3 to interact with the IR (*3*, *9*−*12*) (Figure 1). The importance of flexibility of the insulin molecule for binding to its receptor is underlined by the observation that insulin cross-linked from B29 to A1 is completely inactive although retaining the overall correct fold (*13*). Furthermore mutation of the amino acid residues A2, A19, B23, B24, and B25 has been proven to be the very disruptive toward binding (*14*−*16*).

[†]K.S.T. was recipient of an Industrial Ph.D. scholarship from the Danish Ministry of Science, Technology, and Innovation.

[‡]Coordinates and structure factors have been deposited in the Protein Data Bank with the accession number 2W44.

*To whom correspondence should be addressed. Phone: (+45) 30759157. Fax: (+45) 44444256. E-mail: hnav@novonordisk.com.

[1]Abbreviations: B17A insulin, insulin where the amino acid residue in position B17 has been mutated to an alanine; BSA, bovine serum albumin; CD, circular dichroism; CHO, Chinese hamster ovary cell line; CR, cysteine-rich domain of IR; Des A1−4 insulin, insulin lacking amino acid residues 1−4 in the A-chain; DMSO, dimethyl sulfoxide; FFC, free fat cell; FnIII, fibronectin III domain of IR; hIR, full-length human insulin receptor; HPLC, high-performance liquid chromatography; ID, insert domain of IR; IEF, isoelectric focusing; IGF-I, insulin-like growth factor I; IGF-II, insulin-like growth factor II; IR, insulin receptor; IR-A, insulin receptor without exon 11; IR-B, insulin receptor with exon 11; L1, leucine-rich domain 1 of IR; L2, leucine-rich domain 2 of IR; MALDI TOF, matrix-assisted laser desorption/ionization time of flight; Midi IR-A, truncated insulin receptor construct without exon 11; Midi IR-B, truncated insulin receptor construct with exon 11; NBD, succinimidyl 6-(*N*-(7-nitrobenz-2-oxa-1,3-diazol-4-yl)amino)hexanoate; NMR, nuclear magnetic resonance; PEG, polyethylene glycol; SDS−PAGE, sodium dodecyl sulfate−polyacrylamide gel electrophoresis; SEC, size exclusion chromatography; SPA, scintillation proximity assay; TLS, translation, libration, screw rotation; UV, ultraviolet; WGA, wheat germ agglutinin.

 Published on Web 06/22/2010

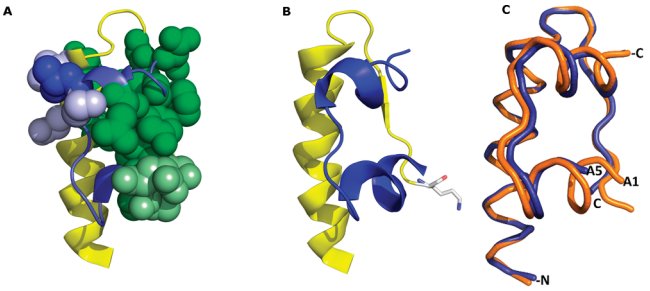

FIGURE 1: Insulin tertiary structure and comparison to the structure of Des A1−4 insulin. (A) Location of the insulin receptor binding sites on the insulin molecule. Site 1 is in light green (residues A1−A4) and dark green (residues A19, B12, B24, B25). Site 2 is in light blue (B17) and dark blue (A13). Human insulin is drawn in *R* conformation in order to facilitate comparison to the experimental Des A1−4 structure. (B) Cartoon representation of insulin (in *R* conformation). The A-chain is in blue and the B-chain in yellow. Lys B29 which is derivatized with the NBD fluorophore is drawn in stick representation. The orientation of the molecule is the same as in (A). (C) Superposition of the C_α atoms of Des A1−4 insulin (blue) with human insulin (PDB entry 1EVR (*57*)) (orange). The N- and C-termini of the A- and B-chains are labeled by their respective residue numbers. The structures were superimposed using the align algorithm in Pymol using the B-chains; the rms deviation between equivalent atoms amounted to 0.25 Å.

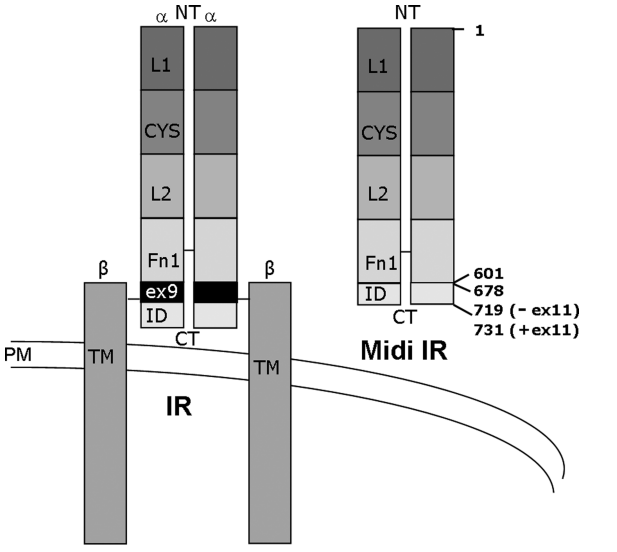

FIGURE 2: Cartoon sketch of the native IR in the membrane and the soluble Midi IR construct used in this paper. The IR entails two *β*-subunits and two α-subunits. The *β*-subunits consist of a transmembrane domain and an intracellular kinase domain, responsible for signaling. The two extracellular α-subunits bind insulin. The Midi IR receptors essentially consist of the two α-subunits without residues 602−677 including the amino acids encoded by exon 9 linked by the C524−C524 cysteine. The Midi IR-A construct without exon 11 terminates at residue 719 whereas Midi IR-B containing the extra 12 amino acids encoded by exon 11 terminates at residue 731. The relative positions of the two leucine-rich repeat domains (L1 and L2), the cysteine-rich region (Cys), the insert domain (ID), and the first of the fibronectin type III domains (Fn1) are indicated.

The IR is a homodimer consisting of two α- and two *β*-subunits, linked by disulfide bridges. In addition, the IR exists in two isoforms (IR-A and IR-B), with IR-A lacking the 12 extracellular amino acids coded by exon 11. The two isoforms display differences in tissue distribution (*2*) and affinity toward IGF-I and IGF-II (*17*). Each monomer consists of 1351 amino acid residues: 403 amino acid residues within the *β*-subunit make up the intracellular kinase domain, which is involved in the signaling cascade; 23 amino acid residues constitute the transmembrane domain; and the remaining 925 amino acid residues comprising the α-subunit and part of the *β*-subunit form the ectodomain, which is involved in insulin binding (*18*) (Figure 2). The α-subunits can be divided into two homologous leucine-rich repeat domains (L1 and L2) separated by a cysteine-rich region (CR), followed by three fibronectin type III (FnIII) domains and ending in the insert domain (ID), which includes exon 11 in the IR-B isoform (*8*, *19*−*22*). Alanine scanning mutagenesis studies of the ligand binding site of the IR indicate that the binding site structure is not the same in the two isoforms (*23*). These studies on the IR ectodomain have revealed that amino acid residues 1−120 of the L1 domain and the carboxy terminus of the α-subunit including the third FnIII domain and the ID domain are important for binding (*24*−*27*). Cross-linking studies have confirmed interaction between insulin and the IR domain L1 and α-subunit C-terminus (*23*, *28*−*36*) and studies of truncated Midi and monomeric receptor constructs (*30*, *36*−*39*) as well as affinity analysis of truncated IR constructs and a minimized monomeric IR (*30*, *31*, *40*−*42*). These studies suggest that upon ligand binding the IR undergoes conformational changes which allow transphosphorylation of three *β*-subunit tyrosine amino acid residues, which in turn activates the kinase activity and hence the signaling cascade (*2*, *38*).

Schäffer (*7*) proposed a model for binding of insulin to the receptor where one insulin molecule binds to both halves of the extracellular part of the IR. The insulin molecule thereby bridges the two distinct receptor sites, site 1 and site 2, on the two IR monomers. A later revision of the model proposed by De Meyts (*39*) based on the structural work of Ward et al. (*19*−*22*) hypothesizes that in fact insulin site 2 (A13 and B17 and neighboring amino acid residues) binds first to the IR and only then does insulin site 1 interact with the receptor (Figure 1) (*27*, *43*, *44*). Later studies showed that insulin binds to both halves of the IR by cross-linking the two receptor sites on the two receptor halves (*27*, *43*, *44*). Furthermore, recent data emphasize that, for high-affinity insulin binding, receptor sites 1 and 2 on opposite receptor monomers are involved (*18*, *32*).

Recently, a crystal structure of an IR ectodomain construct in complex with two Fabs was published (*21*). This structure revealed that each receptor monomer adopts a folded-over conformation in the form of an inverted V, with one limb formed by the N-terminal L1, CR, and L2 domains and the other by the three fibronectin domains (*21*). Insulin was then docked to the IR crystal structure and a binding model proposed, which is consistent with the model of De Meyts. In this model binding is a two-step process, where insulin site 1 is bound to IR site 1 and insulin site 2 binds to IR site 2. The initial binding process involves movement of the upper part of one IR monomer toward the lower part of the other IR monomer, whereas the second binding process is a low-affinity process and involves conformational changes of the N- and C-termini of insulin (*21*, *63*). This ligand-induced conformational change in the IR has been supported by both circular dichroism (CD) spectroscopic studies (*38*) and fluorescence experiments (*45*), where Lys B29 of insulin was specifically labeled with a fluorescent probe (Figure 1B). The fluorescent probe labeling has been shown to only have a minor impact on the biological activity of insulin (*45*). The fluorescence measurements for binding of B29NBD-labeled insulin to a monomeric IR construct revealed that insulin binds to this receptor construct in a biphasic manner. Furthermore, the B29NBD-labeled insulin was shown to retain the biological

activity of native insulin (*45*). This monomeric construct contains only the *cis* site 1 and not site 2. The study of the IR is complicated since no pure and homogeneous preparation exists. Several truncated receptors consisting of the dimeric or monomeric part of the extracellular domain have been expressed, purified, and characterized (*7*, *38*, *39*, *41*). However, they all bind insulin with low nanomolar affinity corresponding to only one site binding. The Midi IR is the only model compound which has high-affinity insulin binding corresponding to interaction with both receptor halves (*39*).

We describe here a fluorescence study of the binding of three fluorophore NBD-X-labeled insulins (NBD-insulin) to both isoforms of purified soluble high-affinity IR constructs, Midi IR-A (−exon 11) and Midi IR-B (+exon 11), which bind insulin with picomolar affinity unlike other purified IR truncations described (*26*, *31*). The study includes NBD-insulin and an insulin analogue mutated in part of binding site 1, NBD-Des A1−4 insulin (Figure 1A, light green spheres). Further, NBD-insulin mutated in binding site 2, NBD-B17A insulin (Figure 1A, light blue spheres), is included. The data show that initial binding of insulin to IR occurs through interactions with insulin site 2 followed by a slower, rate-limiting, interaction between insulin site 1 and the IR. The latter interaction is most likely explained by a conformational change of the initial complex, which is also observed in near-UV CD spectroscopy. Moreover, the presence of the amino acids encoded by exon 11 in Midi IR-B is found to influence insulin site 1 interactions.

MATERIALS AND METHODS

Expression and Purification of Truncated Insulin Receptor. Two Midi IR constructs (Midi IR-B which included IR exon 11 and Midi IR-A which did not) consisting of the α-subunits of the IR dimer without residues 602−677 including exon 9 were prepared by PCR and stably expressed as soluble receptors in CHO Lec 8 cells as described previously (*39*). The Midi IR-A and Midi IR-B, containing the FLAG epitope for purification, were concentrated using 50 mL of anti-FLAG M2-agarose affinity gel from Sigma (A-2220) and eluted with 100 μg/mL Flag-octapeptide (DYKDDDDK) in TBS (50 mM Tris, 150 mM NaCl, pH 7.8). The preparations were then concentrated by ultrafiltration with an Amicon YM10 ultrafiltration disk before the monomeric and dimeric receptor constructs were separated on a Sephadex S300 column in 0.2 M Tris and 0.01% azide, pH 7.8. All purification and storage were at 4 °C, and the purity of the final dimer preparations was evaluated by SDS−PAGE, IEF, and analytical size exclusion chromatography (Figure 3). An extinction coefficient of ε_{278nm} = 94140 M^{-1} cm^{-1} was calculated as described previously (*46*) and used for quantification of both Midi IR-A and Midi IR-B.

Preparation and Purification of NBD-Labeled Insulin Analogues. Insulin labeled with NBD-X (succinimidyl 6-(*N*-(7-nitrobenz-2-oxa-1,3-diazol-4-yl)aminohexonoate; Molecular Probes) and unlabeled B17A insulin have previously been described (*7*, *14*, *45*). For the preparation of Des A1−4 insulin, the analogue A4K insulin was made as previously described (*14*). After expression and purification, this analogue was processed by *Achromobacter lyticus* protease cleavage. The resultant Des A1−4, Des B30 insulin (here called Des A1−4 insulin) was purified via HPLC.

The purified Des A1−4 and B17A insulins were selectively labeled at B29K with the amino specific probe NBD-X. For this

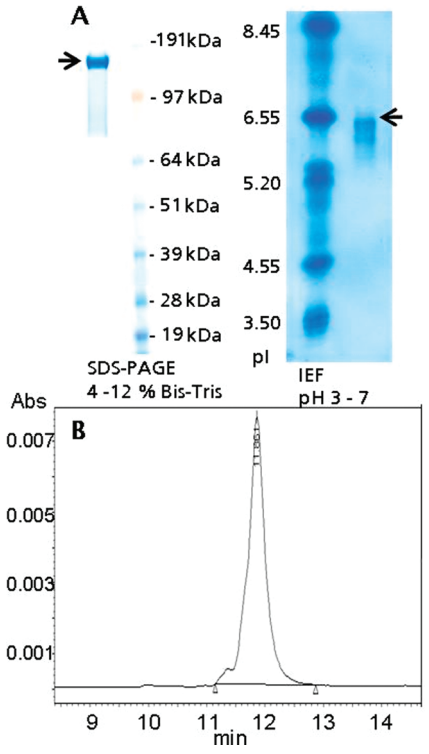

FIGURE 3: Representative analysis of purified Midi IR. Midi IRs were purified by FLAG affinity chromatography followed by gel filtration on a S300 Sephadex column. (A) SDS−PAGE and IEF of purified Midi IR-B. (B) Analytical size exclusion chromatography of purified Midi IR-B. The final preparation consists of homogeneous dimeric truncated insulin receptor.

labeling the insulin was dissolved in 1 M $NaHCO_3$ and mixed with NBD in DMSO in a ratio of 1:3 (mol/mol). The reaction mixtures were incubated at room temperature, and the formation of the derivatized analogue was monitored by HPLC (Waters, Denmark). The reactions were stopped by the addition of 0.2 M ethanolamine. The derivatized insulin analogues were then purified by HPLC using an isocratic elution with an aqueous acetonitrile solvent system containing 0.2 M Na_2SO_4. The purity of selected fractions was verified by MALDI-TOF (Autoflex II TOF/TOF; Bruker Daltonics GmbH, Germany), analytical reverse-phase HPLC, and size exclusion chromatography as described previously (*11*). Finally, confirmation of the attachment to Lys B29 was achieved by N-terminal sequencing and quantification performed by size exclusion chromatography using the extinction coefficient ε_{478nm} = 24100 M^{-1} cm^{-1} (*45*).

Crystal Structure Determination of Des A1−4 Insulin. Crystals were grown by the hanging drop method. To 1 μL of solution (containing 4.4 mg/mL insulin variant Des A1−4 insulin, 260 μM zinc acetate (corresponding to 2.3 Zn per insulin hexamer), 20 mM resorcinol, and 20 mM Tris buffer, pH 7.5) was mixed 1 μL of a reservoir solution (150 mM Na/K-phosphate, pH 7.0, and 7.5% (v/v) ethanol) and equilibrated against the reservoir solution. Crystals grew to a size of ca. 0.2 mm within 1 week.

For data collection a crystal was first cryoprotected in a reservoir solution containing 25% ethylene glycol and then mounted in a nylon loop and frozen in liquid nitrogen. The data were collected on the synchrotron beamline I911-3 of Maxlab (Lund, Sweden) (*47*) at a wavelength of 1 Å using a MarCCD detector (Mar Research, Hamburg). The data were integrated and scaled using XDS and XSCALE (*48*). Analysis of the Matthews coefficient indicated the presence of three insulin

Table 1: Details of Data Collection and Refinement for the Des A1−4 Insulin Crystal

data collection	
space group	$C222_1$ (no. 20)
cell parameters	
a, *b*, *c* (Å)	41.05, 88.62, 73.76
α, *β*, *γ* (deg)	90.0, 90.0, 90.0
resolution range (highest resolution shell) (Å)	40.0−2.0 (2.05−2.00)[e]
total no. of reflections	46876 (1922)
no. of unique reflections	8262 (378)
$I/\sigma I$	24.1 (7.0)
completeness (%)	87.6 (53.5)
R_{merge} (%)[a]	3.9 (19.8)
refinement	
reflections used in refinement	
resolution range	28.3−2.0
no. of used reflections	7800
selected for R_{free}	461
R_{cryst}[b]/R_{free}[b] (%)	20.6/25.8
no. of protein atoms	1140
no. of heteroatoms	26
no. of water molecules	49
average *B*-factors[c] (Å^2)	
main chain atoms	46.5
side chains and water	49.5
rms deviations[d]	
bond lengths (Å)/bond angles (deg)	0.02/1.77
PDB accession code	2w44

[a] $R_{merge} = \sum|I_i - I|/\sum I$, where I_i is an individual intensity measurement and I is the mean intensity for this reflection. [b] R_{cryst} = crystallographic *R*-factor = $\sum||F_o| - |F_c||/\sum|F_o|$, where F_o and F_c are the observed and calculated structure factors, respectively. R_{free} value is calculated in the same way as R_{cryst} but calculated on 5% of the data not included in the refinement. [c] *B*-overall as calculated with TLSANL (66). [d] Root-mean-square deviations of the parameters from their ideal values. [e] Values in parentheses are for the highest resolution shell.

monomers in the asymmetric unit. The structures were solved by molecular replacement with PHASER (*49*) starting from PDB entry 7INS (*50*), which also contains an insulin trimer in the asymmetric unit. The mutated amino acids of the A-chain (A1−4), ligand, and water atoms of the search model were removed prior to the molecular replacement calculations, so that the search model consisted only of protein and zinc atoms. These structures were refined using Refmac (*51*). Refinement of the positional parameters and individual isotropic *B*-factors was alternated with cycles of model building using Coot (*52*). Ligands and metal ions were added when there was convincing electron density in $F_o - F_c$ and $2F_o - F_c$ maps, and where electron density was weak, no model was built, for example, for some of the terminal parts of the B-chain and for amino acid residues Phe 1 and Lys 29 in chain D and Phe 1 in chain F. In order to model anisotropic displacement parameters TLS (translation, libration, screw rotation), tensors for each individual protein chain were refined (*53*) in the final cycles. Water molecules were added using the find water algorithm in Coot. Statistics for data collection and refinement are summarized in Table 1.

Ligand Binding Assays. Two ligand binding assays were performed in which the ability of the insulin analogues to displace radioactively labeled ^{125}I-insulin from the receptors was measured by competition. In the first assay, the polyethylene glycol (PEG) precipitation assay, bound ^{125}I-insulin was measured by PEG precipitation of the receptors as described by Brandt et al. (*39*). In the second and more practical assay, the scintillation proximity assay (SPA), bound ^{125}I-insulin was measured by the scintillation of receptor-coated SPA beads bound to the IR antibody, IR83-7, as described (*54*). Sources of receptors were either Triton X-100-solubilized and WGA-purified full-length human insulin receptors (hIR-A and hIR-B) from recombinant BHK cells or cell supernatants from recombinant CHO Lec8 cells expressing the Midi A or Midi B constructs.

Free Fat Cell Assays. A functional assay in mouse adipocytes (*55*) was employed to estimate the potency of insulin, B17A insulin, Des A1−4 insulin, and all of their NBD derivatives. The assay measured [2-^{3}H]glucose uptake and hence indicated whether the tested insulin analogue could induce intracellular signaling leading to glucose incorporation (*55*). The assay does not allow distinction between IR isoforms, but IR-B is the dominant form in mouse adipocytes. Glucose uptake induced by human insulin was set to 100%, and the biological potency was determined to be the ability of the tested insulin analogues to induce [2-^{3}H]glucose uptake (*55*).

Fluorescence Measurements, Stoichiometry, and Off-Rate Analyses. All steady-state fluorescence measurements were performed with NBD-labeled insulin analogues using a Perkin-Elmer LS-50B luminescence spectrophotometer (Perkin-Elmer Limited, U.K.) essentially as described (*45*). In titration experiments the excitation wavelength was set to 470 nm, and emission spectra were collected at 490−650 nm with a scan speed of 200 nm/min. The cuvette contained 250 nM NBD-labeled insulin analogue, and aliquots of concentrated Midi IR-A and Midi IR-B were added to the cuvette and spectra recorded between each addition. The stoichiometry was determined by plotting intensity at emission maximum (530 nm) as a function of relative receptor concentration. For the assessment of the off-rate the fluorescence intensity at 530 nm, which is the fluorescence emission maximum of the probe, was recorded as a function of time. The off-rate was followed after mixing of a preformed NBD-insulin−receptor complex (0.25 μM NBD-insulin, 0.5 μM Midi IR-A or Midi IR-B) with excess concentrations of B10D, B28D insulin. As previously described (*45*) B10D, B28D insulin has a mutated dimerization interface and was employed to avoid potential perturbations of fluorescence due to insulin dimerization with either of the NBD-insulin analogues. All titrations were carried out in 25 mM Tris, pH 7.8 at 25 °C, and only a very little part of the amplitude (~2%) was lost as a result of the manual mixing. The dissociation curves were fitted to mono- and biphasic decay functions and evaluated by examining the residual plots for all fits.

Near-UV CD Measurements. Near-UV CD spectra were recorded with a Jasco J-715 spectropolarimeter (Jasco Scandinavia AB) calibrated with (1*S*)-(+)-camphor-10-sulfonic acid. All samples were prepared in 25 mM Tris-HCl, pH 7.8, and measured in the near-UV range (250−350 nm) at 20 °C using a 10 mm light path. CD spectra of insulin in the relevant concentrations were subtracted from the spectra of a titration series of insulin−receptor complexes. Subsequently, the spectra were normalized to the molar concentration of receptor protein. Since the extinction coefficient of the Midi IR receptor constructs is 15 times larger than that of the added insulin, the observed changes in the resulting near-UV CD spectra are expected to originate from altered surroundings of the aromatic amino acid residues in the receptor and not from the insulin.

Stopped-Flow Fluorescence Measurements. The dead time of the PiStar 180 stopped-flow apparatus as set up for fluorescence monitoring (Applied Photophysics Limited, Leatherhead, U.K.) was determined to be ca. 1.2 ms via a fluorescence reaction between *N*-bromosuccinamide and *N*-acetyltryptophanamide (*56*).

Table 2: Binding Affinity and Biological Activity of Insulin Analogues[a,b]

	IR-A	IR-B	Midi IR-A	Midi IR-B	FFC[e] (%)
K_d of insulin (pM)	17 ± 4[c]	ND[g]	10 ± 3[d]	10 ± 5[d]	
ligand relative affinity[f]					
insulin	100	100	100	100	100
B17A insulin	43 ± 1	36 ± 3	96 ± 19	107 ± 21	39
Des A1−4 insulin	0.014 ± 0.001	0.015 ± 0.003	0.040 ± 0.006	0.037 ± 0.001	0.02

[a]All parameters were calculated from IC_{50} values based on three replicate experiments and shown as averages ± standard derivations. [b]Triton X-100-solubilized full-length receptors. [c]From Brandt et al. (*40*). [d]K_d determined in polyethylene glycol (PEG) precipitation competition assays. [e]Percent glucose uptake in free fat cells induced by addition of insulin analogues to mouse adipocytes. Human insulin response is set to 100%. [f]Relative affinities determined in scintillation proximity assays (SPA). Human insulin is set to 100. The relative affinities are calculated from IC_{50} values. [g]ND, not determined.

A xenon lamp was employed using entrance and exit slits of 5 mm. The excitation wavelength was set to 470 nm, and the fluorescence signal was filtered out with a cutoff filter at 495 nm. The reaction was followed for 5 s after mixing, and 2000 data points were collected. In the fluorescence time course measurements for formation of complexes between Midi IR-A or Midi IR-B and NBD-B17A insulin or NBD-Des A1−4 insulin were recorded, concentrations of 1 μM Midi IR-A or Midi IR-B and excess amounts (5−40 μM) of B29NBD-labeled insulin analogue were used so as to provide pseudo-first-order conditions. All experiments were carried out in 25 mM Tris-HCl, pH 7.8 at 25 °C, and using a reaction cell with a 10 mm light path. The fluorescence traces for complex formation between insulin and Midi IR-A or Midi IR-B were fit by a non-least squares regression analysis to the sum of two exponentials in eq 1:

$$F_t = F_1[\exp(-t/\tau_1)] + F_2[\exp(-t/\tau_2)] + C \qquad (1)$$

where t is time and F_t represents the fluorescence at time t, $1/\tau_1$ and $1/\tau_2$ correspond to the observed rates for the two phases, F_1 is the fluorescence amplitude of the initial phase, F_2 is the fluorescence amplitude of the second phase, and C is the fluorescence baseline. When appropriate, only a single exponential was used to fit the data.

Data Fitting. All data fitting was performed with GraphPad Prism version 5.00 for Windows, GraphPad Software, San Diego, CA.

RESULTS

Midi IR and Insulin Analogue Purification. Insulin and the B17A insulin and Des A1−4 insulin were successfully expressed in yeast and purified by HPLC. The NBD-labeled analogues NBD-insulin, NBD-B17A insulin, and NBD-Des A1−4 insulin were chemically labeled and HPLC purified. All analogues were of expected mass and purity as measured by mass spectroscopy and analytical HPLC, respectively (data not shown).

Insulin receptor constructs Midi IR-A (−exon 11) and Midi IR-B (+exon 11) were successfully purified by affinity and gel filtration chromatography (Figure 3). The Midi IR receptors displayed affinity for insulin comparable to solubilized whole receptor affinity (Table 2), making them suitable as models for extracellular binding.

Des A1−4 Insulin Structure Determination. To ensure that the deletion of the first four amino acids of the insulin A-chain in the Des A1−4 insulin analogue results in a properly folded protein molecule, we solved the crystal structure of this analogue (Table 1, Figure 1C). Des A1−4 insulin could be crystallized in complex with zinc and resorcinol, resulting in an insulin hexamer in R6 conformation. The crystals belonged to the orthorhombic space group $C222_1$ with one insulin trimer in the asymmetric unit. The complete insulin hexamer is then created by application of a 2-fold crystallographic symmetry operation. The deletion of the four N-terminal amino acids of the A-chain has no significant influence on the overall structure of the insulin molecule: when compared to human insulin in R6 conformation (PDB entry 1EVR (*57*)), the main chain fold is basically identical (Figure 1C). The deletion of amino acid residues A1−4 shortens the first α-helix of the A-chain by one turn. While this has no influence on the overall conformation of the remainder of the molecule, this prompts a change of some of the side chain conformations; most notably Tyr A19 which now occupies the space where Ile A2 is seen in the wild-type structure.

The C-terminus of one of the B-chains contained in the insulin trimer deviates from the typical insulin fold, such that it is no longer in the extended conformation but instead interacts with the (shortened) N-terminus of the A-chain of a neighboring hexamer in the crystal. Consequently, the typically observed antiparallel β-sheet between insulin monomers is not formed (in one out of three dimers). This is presumably due to crystal lattice interactions, and thus we do not expect this conformation to be representative for the monomeric insulin molecule in solution. In summary, the deletion of amino acid residues A 1−4 results in a properly folded insulin molecule where binding site 2 is structurally unchanged. The observed structural differences to wild-type insulin are either limited to the immediate vicinity of the deletions or due to the arrangement of insulin hexamers in the crystal.

NBD-insulin Analogues: Biological Activity and Equilibrium Binding to the Insulin Receptor Isoforms. The PEG precipitation assay revealed that insulin binds both Midi IR receptor constructs with low picomolar affinity (Table 2) similar to Triton X-100-solubilized full-length receptors as previously reported (*39*). The relative affinities of the insulin analogues toward full-length and Midi IRs were measured in a scintillation proximity assay (SPA) and are summarized in Table 2. Mutating B17Leu to Ala in B17A insulin slightly affects binding toward full-length receptors (43% for hIR-A and 36% for hIR-B), but the affinity toward Midi IR receptors is unchanged as compared to insulin (96% for Midi IR-A, 107% for Midi IR-B). In contrast, Des A1−4 insulin displays low affinity for all receptor types (< 0.04%; Table 2), thus indicating that amino acid residues A1−4 are critical for the high-affinity binding of insulin to the IR.

Insulin binding to Midi IR-A and Midi IR-B receptors is reduced ~50% by attaching the NBD probe (data not shown). NBD labeling of B17A insulin and Des A1−4 insulin displays a similar relative effect, and it was therefore concluded that NBD labeling does not significantly hamper binding affinity.

The *in vivo* effects of mutating Leu B17 to Ala in B17A insulin and removing amino acid residues A1−4 in Des A1−4 insulin

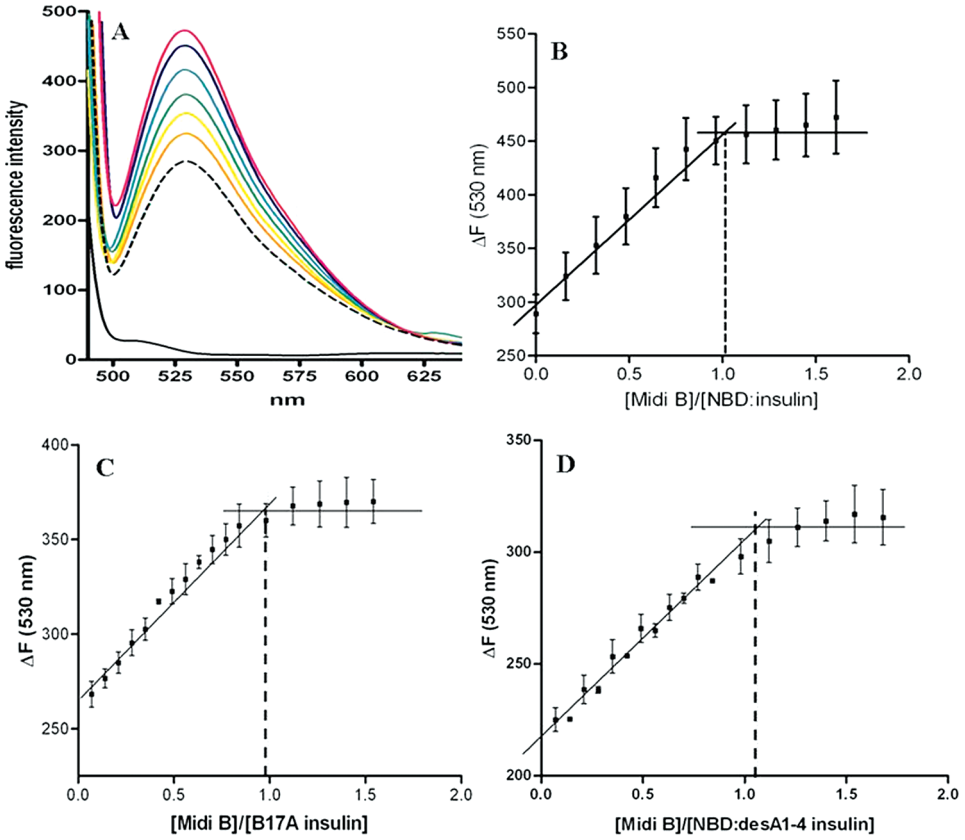

FIGURE 4: Fluorescence change of NBD-labeled insulin in the presence of Midi IR-B. (A) Emission spectra of 250 nM NBD-labeled insulin in the absence of Midi IR-B (orange line) and the increases in fluorescence resulting from sequential addition of up to 720 nM Midi IR-B (colored lines). The broken line shows the spectrum after displacement of NBD-labeled insulin with 50 μM HB10D, PB28D insulin. The black line shows the emission of 25 mM Tris, pH 7.8. (B) Fluorescence enhancement at 530 nm as a function of titration of 250 nM NBD-insulin, (C) NBD-B17A insulin, and (D) NBD-Des A1−4 insulin with sequential addition of Midi IR-B. ΔF is fluorescence measured at 530 nm. As indicated by the dotted lines, the fluorescence saturates at a stoichiometry of 1 to 1.

and derivatizing the insulin analogues with NBD were evaluated in a free fat cell assay, which measured the ability of the various insulins to induce [2-^{3}H]glucose uptake in isolated mouse adipocytes, where the IR-B isoform of the receptor is predominant. Insulin-induced glucose uptake was set to 100%. The corresponding values for B17A insulin and Des A1−4 insulin were 39% and 0.02%, respectively. NBD-labeled insulin retains 32% of its biological activity as compared to insulin (data not shown). Furthermore, the relative activity of the B17A insulin and Des A1−4 insulin with or without the NBD fluorophore attached displays the same order of activity as compared to the equivalent insulin (data not shown). These results suggest that while the NBD fluorophore lowers the biological activity of the insulin, the relative effects of the mutations on the activity are unchanged.

Steady-State Fluorescence Measurement of Stoichiometry of Formation of Complexes between NBD-insulin Analogues and Midi IR-A or Midi IR-B. Figure 4A depicts the spectral changes when titrating NBD-insulin with increasing amounts of Midi IR-B. The fluorescence intensities of the unbound NBD-labeled analogues varied (Figure 4B−D), with NBD-Des A1−4 insulin having the lowest emission intensity. This could be explained by the lack of presumed interactions between the probe and the N-terminal of the A-chain, which is deleted in this analogue (compare panels A and C of Figure 1), thus exposing the probe to a more hydrophilic environment. The binding stoichiometries of the insulin analogues to Midi IR-A and Midi IR-B were determined. To this end the fluorescence change of the NBD insulin analogues upon binding to the Midi IR receptors was followed in a titration experiment (Figure 4). Saturation resulted in an ~60% increase in the quantum yield of the NBD fluorophore for NBD-insulin, ~40% for NBD-B17A insulin, and ~50% for NBD-Des A1−4 insulin.. The fluorescence emission maximum of NBD-insulin (Figure 4A) indicates that the label resides in a hydrophobic environment, consistent with the label being sensitive to the changes in environment on insulin binding to its receptor (*45*). Similar observations were made for NBD-B17A insulin and NBD-Des A1−4 insulin (data not shown). Titrations of NBD-insulin analogues with Midi IR-B are illustrated in Figure 4. A linear increase in fluorescence with concentration of IR is observed until saturation is reached at approximately one molecule of insulin per molecule of IR. Furthermore, fluorescence enhancement induced by the formation of the IR−insulin complex can be completely reversed by displacing the NBD-insulin by adding a large excess (200 times) of unlabeled insulin (HB10D, PB28D insulin), thus indicating that the NBD-insulin is replaced and that complex formation is reversible. In a similar fashion, a stoichiometry of approximately 1:1 is found for all NBD-insulin analogues and both Midi IR-A and Midi IR-B (data not shown). K_d for the binding cannot be determined from this experiment since the lower detection limit is several magnitudes above the K_d = 10 pM measured for insulin.

CD Spectroscopy of IR−Insulin Complex. To explore possible conformational changes upon complex formation of insulin and Midi IR, near-UV CD spectra were recorded in the

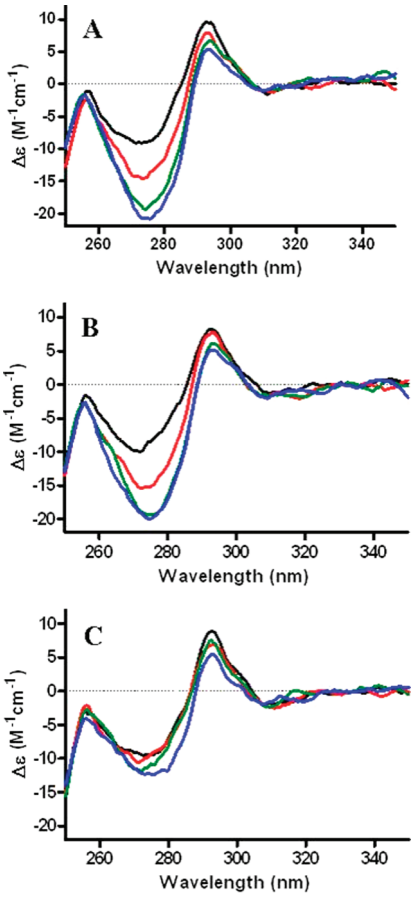

FIGURE 5: CD spectra in the near-UV region of Midi IR-B complexed with (A) insulin, (B) B17A insulin, and (C) Des A1−4 insulin. The black trace shows the spectrum of 2.8 μM uncomplexed Midi IR-B. The red, green, and blue traces show complexes with 1.4, 2.8, and 5.6 μM insulin, respectively, after subtraction of the contribution from insulin.

absence or presence of 1.4, 2.8, and 5.6 μM insulin analogue per 2.8 μM Midi IR. The approximate K_d for binding to the Midi IRs was calculated from the relative affinities in Table 2. Des A1−4 insulin binds with about 4 nM and B17A with about 10 pM to the Midi IRs. The used insulin analogue concentrations were orders of magnitudes larger than these K_d values, thus ensuring full saturation of the binding sites on both Midi IR-A and Midi IR-B. Changes in the near-UV range mainly reflect the environment of aromatic side chains and could be a result of IR−insulin complex formation and/or conformational changes. Spectra were collected for Midi IR-A and Midi IR-B in the presence or absence of insulin, B17A insulin, and Des A1−4 insulin. No differences in near-UV spectra between Midi IR-A and Midi IR-B could be observed, indicating that the exon 11 encoded amino acid residues in Midi IR-B do not cause large structural differences as compared to Midi IR-A (data not shown).

Addition of insulin or B17A insulin to the IR causes large changes in the near-UV spectra for both Midi IR-A (data not shown) and Midi IR-B (Figure 5), and these changes reach saturation at approximately 2.8 μM insulin (Figure 5), thus confirming the 1:1 complex formation observed using fluorescence measurements (Figure 4B). Binding of Des A1−4 insulin to both Midi IR-A (data not shown) and Midi IR-B (Figure 5C) causes only very small spectral changes, indicating that the binding of this analogue does not induce any significant structural changes in the Midi IR receptors (Figure 5C).

Dissociation of the Complexes Formed between NBD-insulin Analogues and Midi IR-A or Midi IR-B. The dissociation of labeled insulin from both receptor constructs was evaluated by adding excess HB10D, PB28D insulin to the IR−insulin complex and following the fluorescence decay (Figure 6). The time courses obtained fit to monophasic exponential decay functions, as evidenced by the random scatter of the residuals (not shown). The fit is not improved by adding a second exponential. From a series of experiments with varying concentration of insulin, Midi IR receptor, and HB10D, PB28D insulin the rate constants were determined and found in the case of NBD-insulin dissociation from Midi IR-A and Midi IR-B to be 0.01 ± 0.007 s^{-1} and 0.01 ± 0.003 s^{-1}, respectively (Table 3). Similar results were obtained with NBD-B17A insulin and NBD-Des A1−4 insulin (Figure 6, Table 3), indicating that insulin is displaced unimolecurlarly and that the rate of dissociation of insulin from the IR is independent of the presence or absence of exon 11.

Stopped-Flow Measurement of Formation of Complexes between NBD-insulin Analogues and Midi IR-A or Midi IR-B. The kinetics of the insulin analogues binding to the IR constructs was studied by measuring the rate of fluorescence enhancement upon binding of NBD-insulin to both Midi IR-A and Midi IR-B. The rates were measured under pseudo-first-order conditions with a constant concentration of 1 μM Midi IR-A or Midi IR-B and mixed with increasing concentrations of NBD-labeled insulin (3−40 μM).

Binding of NBD-insulin to both Midi IR-A and Midi IR-B yielded fluorescence traces that can be described by two distinct phases: an initial phase with large positive amplitude followed by a second slower phase with a relatively small negative amplitude (Figure 7). The data indicate that the insulin−IR complex formation is not dependent on the presence of exon 11. The fluorescence traces for binding of NBD-B17A insulin (mutated in site 2) to both Midi IR-A and Midi IR-B are substantially different from those obtained for NBD-insulin binding. Apparently, they have significantly smaller amplitudes. However, since the fluorescence enhancements upon binding are similar for both NBD-insulin and NBD-B17A insulin (see Figure 4), it is reasonable to assume the initial steep increase in fluorescence is lost in the instrument dead time when B17A insulin binds to the Midi IR receptors. The second slower phase with the small negative amplitudes is, however, still observed (Figure 7).

For both receptor isoforms, Des A1−4 insulin exhibits a fast phase comparable to that of NBD-insulin. When NBD-Des A1−4 insulin binds to Midi IR-A, a second phase with negative amplitude can be observed but with apparently much longer half-life and slightly larger amplitude (Figure 7A) than in the case of NBD-Insulin. Coversely, mixing NBD-Des A1−4 insulin and Midi IR-B results in fluorescence traces that are adequately described by a monophasic exponential function. Hence, the binding of NBD-Des A1−4 insulin does not appear to involve a second phase (Figure 7B).

Kinetic Mechanism for Binding of NBD-insulin to Midi IR-A and Midi IR-B. The stopped-flow fluorescence traces obtained by mixing NBD-insulin with Midi IR receptors can be adequately described by two exponential phases with the assumption that insulin binds the receptor sequentially through interaction from site 1 and site 2. Thus, a plausible model for interpretation of the data is that the initial binding is a bimolecular reaction where molecule A meets molecule B, followed by

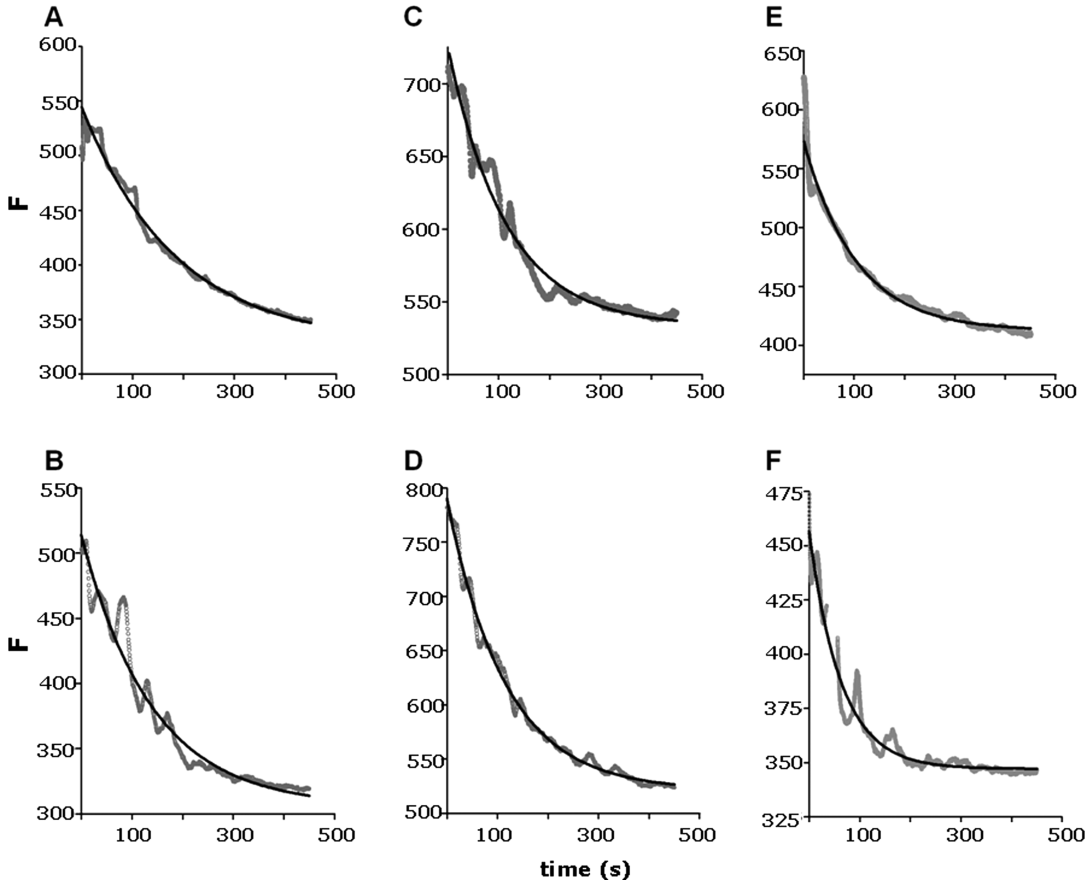

FIGURE 6: Representative time courses for the dissociation of the NBD-labeled insulin−Midi IR-B complex. *F* is the fluorescence intensity measured at 530 nm. The decrease in fluorescence at 530 nm (gray lines) following the displacement of 0.25 μM (A) NBD-insulin, (B) NBD-B17A insulin, or (C) NBD-Des A1−4 insulin from 0.5 μM Midi IR-A and (D) NBD-insulin, (E) NBD-B17A insulin, or (F) NBD-Des A1−4 insulin from 0.5 μM Midi IR-B by the addition of 2.5 μM HB10D, PB28D insulin. The off-rates calculated from the fits (black lines) are given in Table 3.

Table 3: Kinetic Parameters for Interactions between NBD-Labeled Insulin Analogues and Midi IR-A or Midi IR-B[a]

	NBD-insulin		NBD-B17A insulin		NBD-Des A1−4 insulin	
	Midi IR-A	Midi IR-B	Midi IR-A	Midi IR-B	Midi IR-A	Midi IR-B
k_1 (M^{-1} s^{-1})[b]	$4.9 \times 10^6 \pm 0.11$	$3.5 \times 10^6 \pm 0.10$	NA[f]	NA	$1.4 \times 10^5 \pm 1.25$	$1.8 \times 10^5 \pm 0.44$
k_{-1} (s^{-1})[b]	0.001−2	0.001−2	NA	NA	6.28 ± 1.83	2.47 ± 0.71
k_{-2} (s^{-1})[c]	0.01 ± 0.007	0.01 ± 0.003	0.01 ± 0.003	0.01 ± 0.003	0.01 ± 0.008	0.01 ± 0.008
k_2 (s^{-1})[d]	0.96 ± 0.05	0.79 ± 0.03	0.46 ± 0.07	0.20 ± 0.03	NA	NA
K_2[e]	0.012	0.010	0.02	0.05	NA	NA

[a]The model assumes two phases for correct estimation of all relaxation rates. B17A insulin and Des A1-4 insulin are deleted in site 2 and site 1, respectively. [b]Constant determined from linear fit in Figure 8. [c]Constant determined from fit in Figure 6. [d]Constant determined from hyperbolic fit in Figure 8. [e]$K_2 = k_{-2}/k_2$; the constant is without a unit (*62*). [f]NA, not applicable.

an isomerization step, i.e., A + B ⇄ AB ⇄ AB* as shown in eq 2 (*58*):

$$R_2^1 + {}_2^1I \underset{k_{-1}}{\overset{k_1}{\rightleftharpoons}} R_{2.2}^{11}I \underset{k_{-2}}{\overset{k_2}{\rightleftharpoons}} R_{2.2}^{1.1}I \qquad (2)$$

where R is receptor and I is insulin and 1 and 2 indicate the two binding sites present on both insulin and insulin receptor. k_1 (M^{-1} s^{-1}) and k_2 (s^{-1}) are rate constants for the forward reaction, and k_{-1} (s^{-1}) and k_{-2} (s^{-1}) are rate constants for the reverse reactions. The reaction scheme is characterized by two relaxation times, τ_1 and τ_2. Using this data treatment, it is assumed that the step A + B ⇄ AB equilibrates faster than AB ⇄ AB* (*58*). Thus the initial binding phase can be described by the linear eq 3:

$$1/\tau_1 = k_1[\text{NBD-labeled insulin}] + k_{-1} \qquad (3)$$

and the slow binding phase by the hyperbolic eq 4:

$$1/\tau_2 = (k_2[\text{NBD-insulin}]/([\text{NBD-insulin}] + K_1)) + k_{-2} \qquad (4)$$

where $K_1 = k_{-1}/k_1$, and k_{-2} is determined independently from the competitive displacement assay (Table 3).

The expected linear dependence for the initial fast phase and hyperbolic dependence for the second phase can be clearly seen, when the relaxation rate constants for the fast and the slow phase are plotted versus concentration of NBD-insulin (Figure 8A,B). The fits of these data (Table 3) indicate that during the first phase the overall NBD-insulin association with the two Midi IR isoforms occurs equally rapidly with a k_1 of 4.9×10^6 M^{-1} s^{-1} for Midi IR-A and 3.5×10^6 M^{-1} s^{-1} for Midi IR-B.

The linear fit does not allow for reliable determination of k_{-1}, as a range of k_{-1} values were evaluated in the equation and

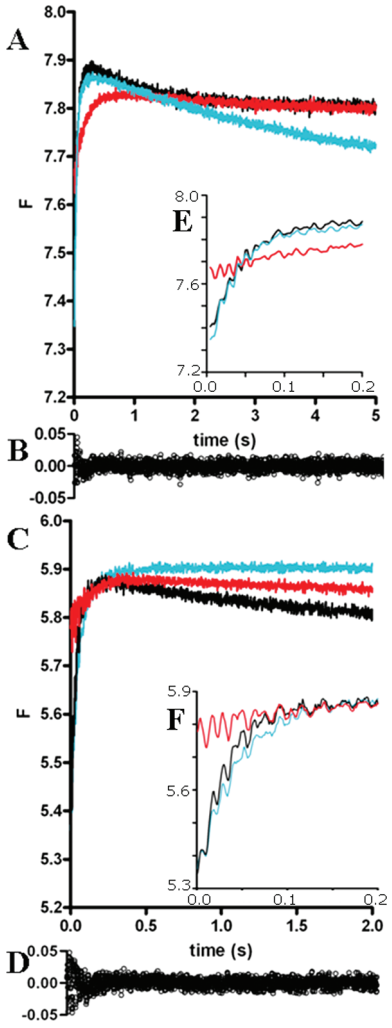

FIGURE 7: Representative time courses of the fluorescence enhancement from rapid mixing of 1 μM Midi IR-A or Midi IR-B and 10 μM NBD-labeled insulin analogue. NBD-insulin (black traces), NBD-B17A insulin (red traces), or NBD-Des A1−4 insulin (blue traces) and (A) Midi IR-A or (C) Midi IR-B. *F* is fluorescence intensity. Measurements were made with a cutoff filter of 495 nm applied. All fluorescence traces for binding of Midi IR-A or Midi IR-B and NBD-insulin were fit to a biphasic exponential expression. (B, D) Residual plot of fit for kinetic traces of NBD-insulin binding. (E, F) The insert depicts the first 0.2 s of the fluorescence traces in (A) and (C).

numbers from 0.001 to 2 s^{-1} all resulted in similar R^2 values, implying that k_{-1} cannot be unambiguously determined. This is a result of the experimental setup with pseudo-first-order conditions using a large excess of insulin analogues in the micromolar range, thus driving the reaction drastically forward and impeding exact determination of k_{-1}. From the hyperbolic plot, k_2 was calculated to be 0.96 s^{-1} for Midi IR-A and 0.79 s^{-1} for Midi IR-B. K_2 was calculated as k_{-2}/k_2 and was 0.012 for Midi IR-A and 0.010 for Midi IR-B (Table 3).

The fluorescence traces for B17A insulin binding to Midi IR-A and Midi IR-B reveal an altered initial binding, resulting in a τ_1 much faster than the 1.2 ms apparatus dead time. Calculation of the first phase rate constants k_1 and k_{-1} was thus disabled. The slower second binding phase was, however, retained, and for B17A insulin k_2 was 0.46 s^{-1} and 0.20 s^{-1} for Midi IR-A and Midi IR-B, respectively (Figure 8C,D and Table 3), and from this K_2 was determined to be 0.02 for Midi IR-A and 0.05 for Midi IR-B. The hyperbolic expression (*4*) was used to analyze this second binding phase for both Midi IR-A and Midi IR-B for simplicity, although we note the quality of the fit for Midi IR-B may point to alternative mechanisms for this particular interaction.

The NBD-Des A1−4 insulin analogue exhibits an apparent fast phase slower than that of NBD-insulin binding to the Midi IR-A and Midi IR-B, as evaluated from the fluorescence traces. The rate constant k_1 was 1.4×10^5 M^{-1} s^{-1} for Midi IR-A and 1.8×10^5 M^{-1} s^{-1} for Midi IR-B (Figure 8E,F, Table 3), respectively. The kinetic data indicate that NBD-Des A1−4 insulin binds differently to the two receptor isoforms (Figure 7). For NBD-Des A1−4 insulin the relaxation times for the second binding phase could not be evaluated, as the second part of the binding trace was either linear with respect to time (when binding to Midi IR-B) or saturated significantly earlier than for the binding of NBD-insulin to Midi IR-A (Figure 7).

DISCUSSION

The binding of insulin to the IR involves insulin bridging the two receptor halves (*17*), where insulin site 1 interacts with both the N- and C-termini of the IR (*23*−*26*, *30*−*34*). The receptor monomers adopt a V-shaped conformation, enabling the simultaneous contact of the insulin molecule with both the C-terminus of one receptor half and the N-terminus of the other receptor half (*19*, *21*, *35*). The binding affinity is in the picomolar range, when measured on preparations of receptors in solution. Several partly purified soluble IRs have been described (*36*, *38*, *45*), but only the Midi IR receptors reported by Brandt et al. (*39*) retain this picomolar affinity and are purified to homogeneity, providing an excellent basis for studying extracellular binding events as seen in Figure 3 and Table 2. The present study describes a time-resolved description of insulin binding to the two isoforms of the insulin receptor, Midi IR-A and Midi IR-B.

We investigated the binding of insulin to the two receptor isoforms, IR-A and IR-B (Figure 2). The affinity for both Midi IR-A and Midi IR-B was 10 pM, and derivatizing insulin with NBD resulted in an ~50% lower receptor affinity. This, together with the reduced glucose uptake, most likely results from steric hindrance of insulin binding due to the fluorophore linkage (Table 2). Even though the presence of the NBD fluorophore has an effect on the affinity to IR, it is still reasonable to use the NBD-labeled analogues to represent the *in vivo* situation, as a significant degree of affinity remains.

A number of reports have shown that the insulin−IR complex binding stoichiometry is concentration dependent (*35*, *44*, *59*). At picomolar concentrations insulin binds with a 1:1 stoichiometry to membrane-bound IR; when insulin concentration is increased to 1−100 nM, a second insulin binds and a negative cooperativity is observed. In the present study, where Midi IR-A or Midi IR-B were titrated at nanomolar concentrations with NBD-labeled insulin, we observed a 1:1 binding stoichiometry, with no second insulin binding as shown in Figure 4. Calculations based on a theoretical model for insulin binding (*52*), with relevant adjustments for the Midi IR receptor conditions, also suggest 1:1 stoichiometry (V. Kiselyov, personal communication). The dissociation of NBD-insulin from the receptor upon displacement with an unlabeled analogue was investigated at a range of concentrations of both insulin analogues and receptor. Displacement of NBD-insulin from the receptor was unimolecular, and the dissociation constant was about 0.01 s^{-1} for both receptor isoforms as shown in Figure 6.

The fluorescence traces for insulin binding to the insulin receptor recorded under stopped-flow conditions indicate that the binding event comprises two phases, as observed from a

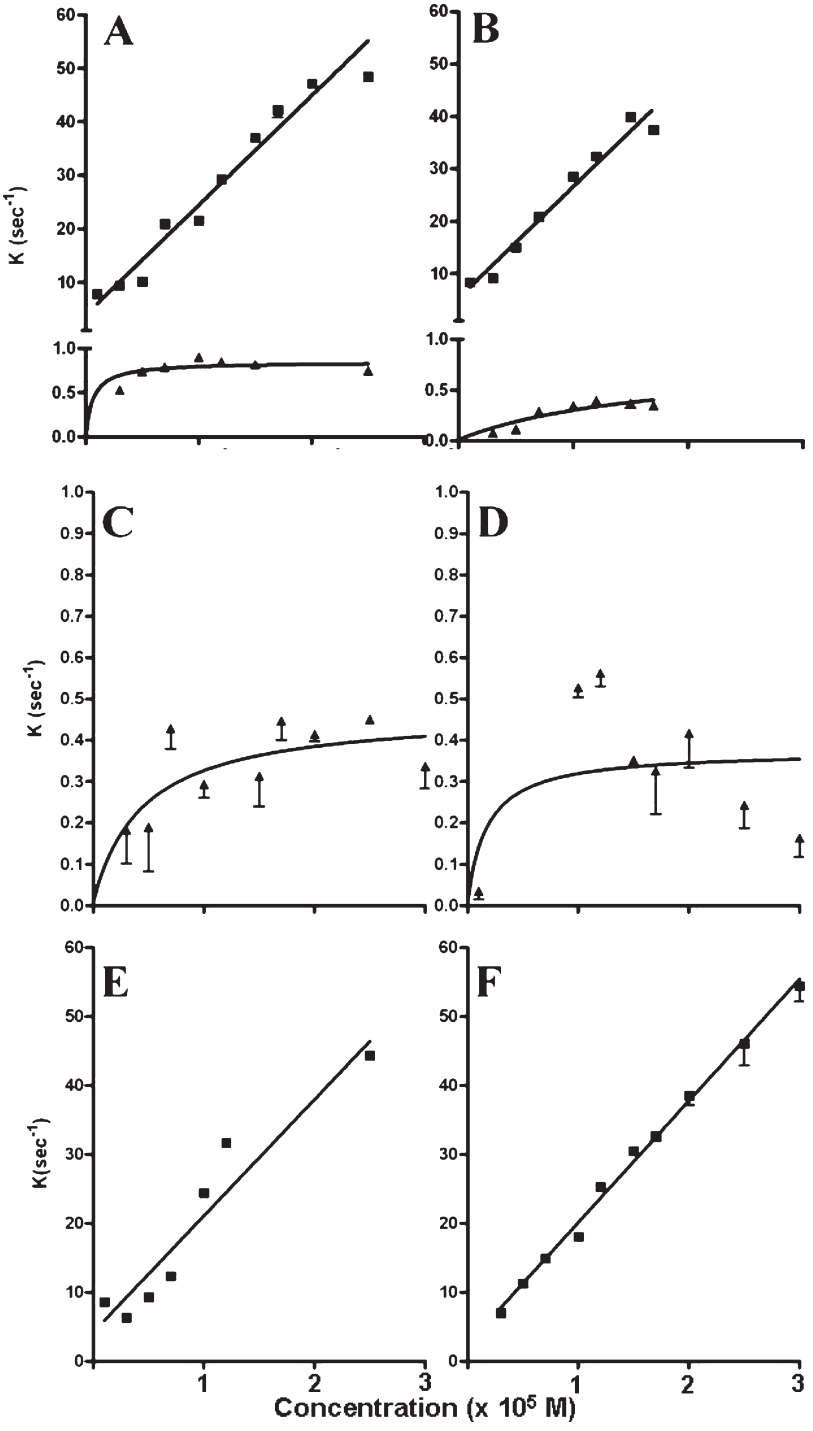

FIGURE 8: Pseudo-first-order rate constants obtained from biphasic exponential fits plotted against concentrations of NBD-labeled insulin. (A, C, E) Midi IR-A association with NBD-insulin, NBD-B17A insulin, and NBD-Des A1−4 insulin, respectively. (B, D, F) Midi IR-B association with NBD-insulin, NBD-B17A insulin, and NBD-Des A1−4 insulin, respectively. Relaxations rates for the fast phases (■) were fitted to the linear equation $1/\tau = k_1$ [B29NBD-labeled insulin] + k_{-1}. Relaxations rates for the slow phases (▲) were fitted to the equation $1/\tau = (k_2$[NBD-insulin])/(K_1[NBD-insulin]) + k_{-2}, where $K_1 = k_{-1}/k_1$. The resulting fits are depicted as full lines.

prominent increase in fluorescence intensity. The first phase is followed by a slow binding phase, with a small negative amplitude (Figure 7). All traces for NBD-insulin fit well to a biphasic exponential expression, exhibiting respectively linear and hyperbolic dependencies on insulin concentration. Initial binding is very fast as evidenced by high k_1 values. Unfortunately, k_{-1} and hence K_d could not be unambiguously determined due to the experimental limitations (Figure 8).

In order to elucidate the binding mechanism, we then included two insulin analogues in the study, one with a partial deletion of site 1, Des A1−4 insulin, and one with a mutated site 2, B17A insulin. Being impaired in one of the two binding sites, B17A insulin and Des A1−4 insulin were not expected to fit to the kinetic model. We chose to delete amino acid residues A1−4 since these site 1 residues are known to be important for IR binding affinity (*60*). The resulting analogue thus retained A19, B12, B24, and B25 of site 1 and an intact site 2. As expected from studies of insulin mutated at A3, this analogue has a severely impaired receptor affinity, resulting in very low potency as determined by glucose uptake in free fat cells. The crystal structure of Des A1−4

insulin reveals that the markedly reduced receptor binding and biological response result from removal of amino acid residues A1−4, since the overall correct fold of the molecule is retained (Figure 1C). Site 1 is therefore a high-affinity binding site. Insulin with a compromised site 2 (B17A insulin), but with an intact site 1 and A13 of site 2, was also included in this study. It has previously been shown that substitution of insulin B17 has little influence on the affinity to full-length IR (*54*). Since A13 and B17 appear to contribute evenly to insulin binding to site 2 (*7*), the B17A insulin can be used to characterize the change of insulin binding as a result of changing site 2. In our hands, B17A insulin and insulin displayed a remarkably similar Midi IR receptor binding, but full-length IR receptor affinity and glucose uptake were lowered with B17A insulin as compared to insulin. The Midi receptor contains the amino acid sequence of the IR site 2, and the high affinity of the Midi receptor to insulin suggests a native receptor conformation. The relative affinities reveal that insulin site 1 is important for the high-affinity binding of insulin to its receptor and site 2 is a low-affinity contribution (Table 2).

The two insulins, B17A insulin and Des A1−4 insulin, were also labeled with the fluorescence probe NBD so as to facilitate fluorescence kinetic studies. The influence on activity of linking the NBD fluorophore to the insulin analogues was examined in both *in vitro* cell-free assays and in free fat cells, and it was concluded that NBD-labeling did not interfere with the effects of the mutations. The displacement of NBD-B17A insulin and NBD-Des A1−4 insulin from Midi IR-A and Midi IR-B was described by a single phase, reflecting a simple dissociation mechanism with a single rate-limiting step, resulting in dissociation rates of about 0.01 s^{-1} similar to that of NBD-insulin. This indicates that both insulin and the two mutant insulin analogues leave the receptor in a similar manner (Figure 6).

As evidenced by the kinetic studies, neither the NBD-B17A insulin nor NBD-Des A1−4 insulin exhibited binding similar to insulin. Given the observed loss of most of the amplitude of the fast phase in the instrument dead time (1.2 ms), it is likely that the first phase of NBD-B17A insulin binding to Midi IR-A or Midi IR-B is significantly faster than that of NBD-insulin. It cannot be ruled out that a third phase occurs within the dead time, but the above explanation is the simplest plausible explanation within the experimental setup. This faster first phase in NBD-B17A insulin binding to Midi IR-A and Midi IR-B indicates that site 2 (B17Leu) is involved in this initial step. The second slow phase is apparently unchanged as compared to NBD-insulin. Thus, insulin binds to the receptor very quickly as evidenced by the kinetic traces. In CD measurements B17A insulin induces conformational changes in the receptor complex which are indistinguishable from those induced by insulin (Figure 5). This indicates that the initial binding event is clearly separated from the second binding event. Therefore, it does not affect the ability to bridge the receptor halves. De Meyts has previously suggested this order of binding, initially site 2 and then site 1 (*27*, *43*, *44*). McKern et al. (*21*) propose the opposite order of binding, where site 1 suggested to be the low-affinity site binds first; then the high affinity is introduced by the second binding of site 2. What we show is that the low-affinity site which is shown to be site 2 binds first to the IR and thereafter the high-affinity site shown to be site 1 binds to the IR and introduces the measured IR conformational change. This binding reaction is illustrated in Figure 9. The previously described insulin N- and C-terminal conformational change (*63*) is therefore likely to occur as part of the second of the binding event.

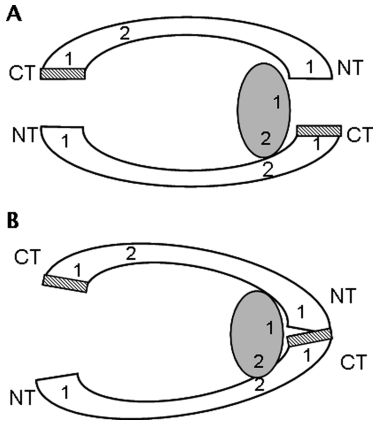

FIGURE 9: Schematic drawing of the binding of one insulin molecule to the IR. The ectodomain of the IR is drawn in the folded over conformation. Here IR-B is depicted with exon 11 highlighted. Insulin is depicted as a circle, where 1 and 2 represent binding sites 1 and 2, respectively. On the basis of our data we suggest a model with two binding steps: (A) Initial binding is fast and occurs between insulin site 2 and site 2 on the IR. (B) The second binding event is slow and involves insulin site 1 interacting with site 1 on the IR. IR site 1 on both IR-A and IR-B is comprised by the N- and C-terminal region on separate monomers. This second binding event is of high affinity and involves conformational change in the insulin−IR complex.

The fluorescence measurements in combination with the CD measurements also show that the second binding phase is crucial for stable receptor−insulin complex formation as Des A1−4 insulin is unable to induce change in tertiary structure of the receptor complex upon binding as seen in Figure 5. Furthermore, when Des A1−4 insulin binds to Midi IR-B, the second binding phase is apparently absent, whereas Des A1−4 insulin binding to Midi IR-A results in a second binding phase with a very slow half-life. The negative amplitude observed in stopped-flow measurements for the second phase of binding between NBD-Des A1−4 insulin and Midi A probably reflects differences in binding site architecture of the two receptor isoforms, as previously reported by Whittaker et al. (*23*). It is unlikely to be a result of a conformational change in the Midi IR-A, since no changes in CD spectra can be observed. Together, these results indicate that A19, B12, B24, and B25 of site 1 are important for binding in the region surrounding exon 11. Furthermore, the lack of the slow binding phase observed with Des A1−4 insulin supports the hypothesis that during the binding event the B-chain of insulin changes conformation, thereby exposing A1−A3 to interact with the receptor (*3*, *9*, *11*, *12*, *15*, *60*, *61*). Recent cross-linking studies confirm interaction between B25/B27 and the IR α-subunit C-terminus (*29*).

Although insulin and B17A insulin have comparable Midi IR affinity, they complex the Midi IR-A and Midi IR-B receptor constructs differently as evidenced by the kinetic experiments, with part of the binding event being absent for B17A insulin binding to Midi IR-A and Midi IR-B. Altering Leu B17 to Ala results in a superfast insulin mutant with a markedly increased k_1 but with an unaffected receptor affinity. The absence of the leucine side chain in B17A insulin may result in a less constrained binding interface and suggests that Leu B17 may be important in ensuring the correct orientation of insulin via slowing the reaction event down. This could also explain why glucose uptake is reduced to 39% with this analogue. Alanine scans of both human growth hormone and its receptor produced examples of increased overall on-rates upon mutation (*64*, *65*)

The larger deletion removing amino acid residues A1−4, and thus most of site 1, results in even more pronounced effects. This is observed as very low receptor affinity (in steady-state measurements), which is consistent with a 30 times lower k_1 and faster k_{-1}, unability to induce conformational changes in the receptor, and a very low biological activity. This illustrates that high-affinity binding is a prerequisite for conformational change of the receptor and eventually for biological activity.

Recent studies with an insulin-mimetic peptide with insulin-like IR affinity revealed a very different signaling from insulin. The peptide was virtually unable to induce Shc and ERK signals, whereas glycogen synthesis was very similar (*62*). Analyzing the B17A insulin-mediated phosphorylation and signaling pattern could shed light on this by potentially linking the insulin binding mode to a specific signaling pattern. Likewise, results for Des A1−4 insulin suggest that the presence of the exon 11 encoded amino acids modulate the manner in which insulin is bound to IR and thus suggest that the two different IR splice variants may relay different (overlapping) signals on insulin binding.

We propose a model for the events taking place during recognition and binding of insulin to its receptor (Figure 9 and eq 2). Initially, and as observed by stopped-flow fluorescence measurements, insulin site 2 (including Leu A17) binds to the receptor site 2 of IR in a fast step, probably involving the FnIII-1 domain of one of the α-subunits. This is followed by a conformational change of the initial complex which is rate limiting. This change probably involves amino acid residues A1−A4 of insulin, since their absence results in both considerably lower binding affinities and the lack of conformational change. As illustrated in Figure 9, we propose that high-affinity binding and conformational change involve the binding of insulin site 1 to the receptor site 1 composed of amino acid residues in the N-terminal (L1) in one receptor half and in the C-terminal (ID domain) of the other half in accordance with the findings of Chan et al. (*18*). In the IR B isoform the additional amino acid residues encoded by exon 11 adjoin the residues in the C-terminal ID domain important for insulin site 1 binding and may influence the second binding event and the conformational change. This may be linked to our finding that Des A1−4 insulin appears to show distinct patterns in the secondary phases.

In summary, we show that insulin binds the IR in two distinct phases: where the initial binding is fast and relates to insulin site 2, and a subsequent, conformational change involving insulin site 1 and the IR site 1 constitutes the second slower phase. The latter binding is the most important for high affinity and may be influenced by the presence of the amino acid sequence encoded by exon 11. Both the initial association and the subsequent rearrangement of the insulin−receptor complex are important for biological activity.

ACKNOWLEDGMENT

We thank Susan Danielsen for technical assistance on the CD measurements. Dr. Andrew James Bernie is thanked for providing outstanding expertise in the proofreading of the manuscript.

REFERENCES

1. White, M. F., and Kahn, C. R. (1994) The insulin signaling system. *J. Biol. Chem. 269*, 1–4.
2. Denley, A., Wallace, J. C., Cosgrove, L. J., and Forbes, B. E. (2003) The insulin receptor isoform exon 11- (IR-A) in cancer and other diseases: a review. *Horm. Metab. Res. 35*, 778–785.
3. Ludvigsen, S., Olsen, H. B., and Kaarsholm, N. C. (1998) A structural switch in a mutant insulin exposes key residues for receptor binding. *J. Mol. Biol. 279*, 1–7.
4. Olsen, H. B., Ludvigsen, S., and Kaarsholm, N. C. (1998) The relationship between insulin bioactivity and structure in the NH_2-terminal A-chain helix. *J. Mol. Biol. 284*, 477–488.
5. Baker, E. N., Blundell, T. L., Cutfield, J. F., Cutfield, S. M., Dodson, E. J., Dodson, G. G., Hodgkin, D. M., Hubbard, R. E., Isaacs, N. W., and Reynolds, C. D. (1988) The structure of 2Zn pig insulin crystals at 1.5 Å resolution. *Philos. Trans. R. Soc. London, Ser. B 319*, 369–456.
6. Derewenda, U., Derewenda, Z., Dodson, E. J., Dodson, G. G., Reynolds, C. D., Smith, G. D., Sparks, C., and Swenson, D. (1989) Phenol stabilizes more helix in a new symmetrical zinc insulin hexamer. *Nature 338*, 594–596.
7. Schaffer, L. (1994) A model for insulin binding to the insulin receptor. *Eur. J. Biochem. 221*, 1127–1132.
8. De Meyts, P., and Whittaker, J. (2002) Structural biology of insulin and IGF1 receptors: implications for drug design. *Nat. Rev. Drug Discovery 1*, 769–783.
9. Hua, Q. X., Shoelson, S. E., Kochoyan, M., and Weiss, M. A. (1991) Receptor binding redefined by a structural switch in a mutant human insulin. *Nature 354*, 238–241.
10. Huang, K., Chan, S. J., Hua, Q. x., Chu, Y. C., Wang, R. y., Klaproth, B., Jia, W., Whittaker, J., De Meyts, P., Nakagawa, S. H., Steiner, D. F., Katsoyannis, P. G., and Weiss, M. A. (2007) The A-chain of insulin contacts the insert domain of the insulin receptor. Photo-cross-linking and mutagenesis of a diabetes-related crevice. *J. Biol. Chem. 282*, 35337–35349.
11. Xu, B., Hu, S. Q., Chu, Y. C., Wang, S., Wang, R. Y., Nakagawa, S. H., Katsoyannis, P. G., and Weiss, M. A. (2004) Diabetes-associated mutations in insulin identify invariant receptor contacts. *Diabetes 53*, 1599–1602.
12. Xu, B., Hua, Q. X., Nakagawa, S. H., Jia, W., Chu, Y. C., Katsoyannis, P. G., and Weiss, M. A. (2002) Chiral mutagenesis of insulin's hidden receptor-binding surface: structure of an allo-isoleucine(A2) analogue. *J. Mol. Biol. 316*, 435–441.
13. Derewenda, U., Derewenda, Z., Dodson, E. J., Dodson, G. G., Bing, X., and Markussen, J. (1991) X-ray analysis of the single chain B29-A1 peptide-linked insulin molecule. A completely inactive analogue. *J. Mol. Biol. 220*, 425–433.
14. Kristensen, C., Kjeldsen, T., Wiberg, F. C., Schaffer, L., Hach, M., Havelund, S., Bass, J., Steiner, D. F., and Andersen, A. S. (1997) Alanine scanning mutagenesis of insulin. *J. Biol. Chem. 272*, 12978–12983.
15. Xu, B., Hu, S. Q., Chu, Y. C., Huang, K., Nakagawa, S. H., Whittaker, J., Katsoyannis, P. G., and Weiss, M. A. (2004) Diabetes-associated mutations in insulin: consecutive residues in the B chain contact distinct domains of the insulin receptor. *Biochemistry 43*, 8356–8372.
16. Nakagawa, S. H., and Tager, H. S. (1992) Importance of aliphatic side-chain structure at positions 2 and 3 of the insulin A chain in insulin-receptor interactions. *Biochemistry 31*, 3204–3214.
17. Denley, A., Brierley, G. V., Carroll, J. M., Lindenberg, A., Booker, G. W., Cosgrove, L. J., Wallace, J. C., Forbes, B. E., and Roberts, C. T., Jr. (2006) Differential activation of insulin receptor isoforms by insulin-like growth factors is determined by the C domain. *Endocrinology 147*, 1029–1036.
18. Chan, S. J., Nakagawa, S., and Steiner, D. F. (2007) Complementation analysis demonstrates that insulin cross-links both {alpha} subunits in a truncated insulin receptor dimer. *J. Biol. Chem. 282*, 13754–13758.
19. Ward, C., Lawrence, M., Streltsov, V., Garrett, T., McKern, N., Lou, M. Z., Lovrecz, G., and Adams, T. (2008) Structural insights into ligand-induced activation of the insulin receptor. *Acta Physiol. (Oxford) 192*, 3–9.
20. Lawrence, L. J., McKern, N. M., and Ward, C. W. (2007) Insulin receptor structure and its implications for the IGF-1 receptor. *Curr. Opin. Struct. Biol. 17*, 1–7.
21. McKern, N. M., Lawrence, M. C., Streltsov, V. A., Lou, M. Z., Adams, T. E., Lovrecz, G. O., Elleman, T. C., Richards, K. M., Bentley, J. D., Pilling, P. A., Hoyne, P. A., Cartledge, K. A., Pham, T. M., Lewis, J. L., Sankovich, S. E., Stoichevska, V., Da, S. E., Robinson, C. P., Frenkel, M. J., Sparrow, L. G., Fernley, R. T., Epa, V. C., and Ward, C. W. (2006) Structure of the insulin receptor ectodomain reveals a folded-over conformation. *Nature 443*, 218–221.
22. Sparrow, L. G., McKern, N. M., Gorman, J. J., Strike, P. M., Robinson, C. P., Bentley, J. D., and Ward, C. W. (1997) The disulfide bonds in the C-terminal domains of the human insulin receptor ectodomain. *J. Biol. Chem. 272*, 29460–29467.

23. Whittaker, J., Sorensen, H., Gadsboll, V. L., and Hinrichsen, J. (2002) Comparison of the functional insulin binding epitopes of the A and B isoforms of the insulin receptor. *J. Biol. Chem. 277*, 47380–47384.
24. Mynarcik, D. C., Williams, P. F., Schaffer, L., Yu, G. Q., and Whittaker, J. (1997) Identification of common ligand binding determinants of the insulin and insulin-like growth factor 1 receptors. Insights into mechanisms of ligand binding. *J. Biol. Chem. 272*, 2077–2081.
25. Mynarcik, D. C., Yu, G. Q., and Whittaker, J. (1996) Alanine-scanning mutagenesis of a C-terminal ligand binding domain of the insulin receptor alpha subunit. *J. Biol. Chem. 271*, 2439–2442.
26. Williams, P. F., Mynarcik, D. C., Yu, G. Q., and Whittaker, J. (1995) Mapping of an NH_2-terminal ligand binding site of the insulin receptor by alanine scanning mutagenesis. *J. Biol. Chem. 270*, 3012–3016.
27. De Meyts, P. (2004) Insulin and its receptor: structure, function and evolution. *BioEssays 26*, 1351–1362.
28. Fabry, M., Schaefer, E., Ellis, L., Kojro, E., Fahrenholz, F., and Brandenburg, D. (1992) Detection of a new hormone contact site within the insulin receptor ectodomain by the use of a novel photoreactive insulin. *J. Biol. Chem. 267*, 8950–8956.
29. Xu, B., Huang, K., Chu, Y., Hu, S., Nakagawa, S., Wang, S., Wang, R., Whittaker, J., Katsoyannis, P. G., and Weiss, M. A. (2009) Decoding the cryptic active conformation of a protein by synthetic photoscanning: insulin inserts a detachable arm between receptor domains. *J. Biol. Chem. 284*, 14597–14608.
30. Hao, C., Whittaker, L., and Whittaker, J. (2006) Characterization of a second ligand binding site of the insulin receptor. *Biochem. Biophys. Res. Commun. 347*, 334–339.
31. Surinya, K. H., Molina, L., Soos, M. A., Brandt, J., Kristensen, C., and Siddle, K. (2002) Role of insulin receptor dimerization domains in ligand binding, cooperativity, and modulation by anti-receptor antibodies. *J. Biol. Chem. 277*, 16718–16725.
32. Whittaker, L., Hao, C., Fu, W., and Whittaker, J. (2008) High-affinity insulin binding: insulin interacts with two receptor ligand binding sites. *Biochemistry 47*, 12900–12909.
33. Whittaker, J., and Whittaker, L. (2005) Characterization of the functional insulin binding epitopes of the full-length insulin receptor. *J. Biol. Chem. 280*, 20932–20936.
34. Mynarcik, D. C., Williams, P. F., Schaffer, L., Yu, G. Q., and Whittaker, J. (1997) Identification of common ligand binding determinants of the insulin and insulin-like growth factor 1 receptors. Insights into mechanisms of ligand binding. *J. Biol. Chem. 272*, 18650–18655.
35. De Meyts, P. (2008) The insulin receptor: a prototype for dimeric, allosteric membrane receptors? *Trends Biochem. Sci. 33*, 376–384.
36. Schaefer, E. M., Siddle, K., and Ellis, L. (1990) Deletion analysis of the human insulin receptor ectodomain reveals independently folded soluble subdomains and insulin binding by a monomeric alpha-subunit. *J. Biol. Chem. 265*, 13248–13253.
37. Benyoucef, S., Surinya, K. H., Hadaschik, D., and Siddle, K. (2007) Characterization of insulin/IGF hybrid receptors: contributions of the insulin receptor L2 and Fn1 domains and the alternatively spliced exon 11 sequence to ligand binding and receptor activation. *Biochem. J. 403*, 603–613.
38. Florke, R. R., Schnaith, K., Passlack, W., Wichert, M., Kuehn, L., Fabry, M., Federwisch, M., and Reinauer, H. (2001) Hormone-triggered conformational changes within the insulin-receptor ectodomain: requirement for transmembrane anchors. *Biochem. J. 360*, 189–198.
39. Brandt, J., Andersen, A. S., and Kristensen, C. (2001) Dimeric fragment of the insulin receptor alpha-subunit binds insulin with full holoreceptor affinity. *J. Biol. Chem. 276*, 12378–12384.
40. Kristensen, C., Wiberg, F. C., Schaffer, L., and Andersen, A. S. (1998) Expression and characterization of a 70-kDa fragment of the insulin receptor that binds insulin. Minimizing ligand binding domain of the insulin receptor. *J. Biol. Chem. 273*, 17780–17786.
41. Andersen, A. S., Kjeldsen, T., Wiberg, F. C., Vissing, H., Schaffer, L., Rasmussen, J. S., De Meyts, P., and Moller, N. P. (1992) Identification of determinants that confer ligand specificity on the insulin receptor. *J. Biol. Chem. 267*, 13681–13686.
42. Andersen, A. S., Kjeldsen, T., Wiberg, F. C., Christensen, P. M., Rasmussen, J. S., Norris, K., Moller, K. B., and Moller, N. P. (1990) Changing the insulin receptor to possess insulin-like growth factor I ligand specificity. *Biochemistry 29*, 7363–7366.
43. De Meyts, P., Palsgaard, J., Sajid, W., Theede, A. M., and Aladdin, H. (2004) Structural biology of insulin and IGF-1 receptors. *Novartis Found. Symp. 262*, 160–171.
44. De Meyts, P. (1994) The structural basis of insulin and insulin-like growth factor-I receptor binding and negative co-operativity, and its relevance to mitogenic versus metabolic signalling. *Diabetologia 37* (Suppl. 2), S135–S148.
45. Schlein, M., Havelund, S., Kristensen, C., Dunn, M. F., and Kaarsholm, N. C. (2000) Ligand-induced conformational change in the minimized insulin receptor. *J. Mol. Biol. 303*, 161–169.
46. Pace, C. N., Vajdos, F., Fee, L., Grimsley, G., and Gray, T. (1995) How to measure and predict the molar absorption coefficient of a protein. *Protein Sci. 4*, 2411–2423.
47. Mammen, C. B., Ursby, T., Cerenius, Y., Thunnissen, M., Als-Nielsen, J., Larsen, S., and Liljas, A. (2002) Design of a 5-station macromolecular crystallography beamline at MAX-lab. *Acta Phys. Pol., A 101*, 595–602.
48. Kabsch, W. (1993) Automatic processing of rotation diffraction data from crystals of initially unknown symmetry and cell constants. *J. Appl. Crystallogr. 26*, 795–800.
49. McCoy, A. J., Grosse-Kunstleve, R. W., Adams, P. D., Winn, M. D., Storoni, L. C., and Read, R. J. (2007) Phaser crystallographic software. *J. Appl. Crystallogr. 40*, 658–674.
50. Balschmidt, P., Hansen, F. B., Dodson, E. J., Dodson, G. G., and Korber, F. (1991) Structure of porcine insulin cocrystallized with clupeine Z. *Acta Crystallogr. B47*, 975–986.
51. Winn, M. D., Murshudov, G. N., and Papiz, M. Z. (2003) Macromolecular TLS refinement in REFMAC at moderate resolutions, Methods in Enzymology, Academic Press, New York.
52. Emsley, P., and Cowtan, K. (2004) Coot: model-building tools for molecular graphics. *Acta Crystallogr. D60*, 2126–2132.
53. Winn, M. D., Isupov, M. N., and Murshudov, G. N. (2001) Use of TLS parameters to model anisotropic displacements in macromolecular refinement. *Acta Crystallogr. D57*, 122–133.
54. Glendorf, T., Sorensen, A. R., Nishimura, E., Pettersson, I., and Kjeldsen, T. (2008) Importance of the solvent-exposed residues of the insulin B chain alpha-helix for receptor binding. *Biochemistry 47*, 4743–4751.
55. Moody, A. J., Stan, M. A., Stan, M., and Gliemann, J. (1974) A simple free fat cell bioassay for insulin. *Horm. Metab. Res. 6*, 12–16.
56. Peterman, B. F. (1979) Measurement of the dead time of a fluorescence stopped-flow instrument. *Anal. Biochem. 93*, 442–444.
57. Smith, G. D., Ciszak, E., Magrum, L. A., Pangborn, W. A., and Blessing, R. H. (2000) Crystallographic characterization of two novel crystal forms of human insulin induced by chaotropic agents and a shift in pH. *Acta Crystallogr., Sect. D: Biol. Crystallogr. 56*, 1541–1548.
58. Bernasconi, C. F. (1976) Relaxation Kinetics, Academic Press, New York.
59. Kiselyov, V. V., Versteyhe, S., Gauguin, L., and De Meyts, P. (2009) Harmonic oscillator model of the insulin and IGF1 receptors binding and activation. *Mol. Syst. Biol. 5*, 243.
60. Huang, K., Chan, S. J., Hua, Q. x., Chu, Y. C., Wang, R. y., Klaproth, B., Jia, W., Whittaker, J., De Meyts, P., Nakagawa, S. H., Steiner, D. F., Katsoyannis, P. G., and Weiss, M. A. (2007) The A-chain of insulin contacts the insert domain of the insulin receptor. Photo-cross-linking and mutagenesis of a diabetes-related crevice. *J. Biol. Chem. 282*, 35337–35349.
61. Xu, B., Hua, Q. X., Nakagawa, S. H., Jia, W., Chu, Y. C., Katsoyannis, P. G., and Weiss, M. A. (2002) A cavity-forming mutation in insulin induces segmental unfolding of a surrounding alpha-helix. *Protein Sci. 11*, 104–116.
62. Jensen, M., Hansen, B., De Meyts, P., Schaffer, L., and Urso, B. (2007) Activation of the insulin receptor by insulin and a synthetic peptide leads to divergent metabolic and mitogenic signaling and responses. *J. Biol. Chem. 282*, 35179–35186.
63. Wan, Z (2004) Enhancing the activity of insulin at the receptor interface: crystal structure and photo-cross-linking of A8 analogues. *Biochemistry 43*, 16119–16133.
64. Cunningham, B. C., and Wells, J. A. (1993) Comparison of a structural and a functional epitope. *J. Mol. Biol. 234*, 554–563.
65. Clackson, T., Ultscha, M. H., Wells, J. A., and de Vos, A. M. (1998) Structural and functional analysis of the 1:1 growth hormone:receptor complex reveals the molecular basis for receptor affinity. *J. Mol. Biol. 277*, 1111–1128.